Thermal cross-track cross talk in phase-change optical disk data storage

Cite as: Journal of Applied Physics **88**, 1214 (2000); https://doi.org/10.1063/1.373806
Submitted: 28 February 2000 . Accepted: 01 May 2000 . Published Online: 14 July 2000

Chubing Peng, and M. Mansuripur

Thermal cross-track cross talk in phase-change optical disk data storage

Chubing Peng[a] and M. Mansuripur
Optical Sciences Center, University of Arizona, Tucson, Arizona 85721

(Received 28 February 2000; accepted for publication 1 May 2000)

We have investigated the temperature distribution in land/groove phase-change optical disks. The incident beam is linearly polarized either parallel to track ($E_{\parallel}$ polarization) or tangential to track ($E_{\perp}$ polarization). Calculations have shown that temperature profiles in the medium are dependent on the wavelength of light, the state of polarization, the geometry of the grooved structure, and the multilayer stack. The temperature profiles are quite different between the land track and the groove track. Thermal cross-track cross talk from a land track to its neighboring groove tracks is higher than that from a groove track to its neighboring land tracks. The interaction between the $E_{\perp}$ electric field and the grooved structure is mainly responsible for thermal cross-track cross talk. © *2000 American Institute of Physics.* [S0021-8979(00)08215-3]

I. INTRODUCTION

In erasable phase-change (PC) optical disk data storage, a focused laser beam is used as a heating source to reversibly switch a micron-sized area in the storage layer between amorphous and crystallize states.[1–3] A short, high power laser pulse increases the local temperature of the storage layer above its melting point. When the pulse ends, the molten spot cools down rapidly, forming an amorphous mark on a crystalline background. The mark can later be identified by using the same focused laser beam at a much lower laser power to detect the reflection (or transmission) of the spot relative to its crystalline surroundings.

In current PC data storage systems, the scheme of land-groove (LG) recording is widely used.[4] In this scheme, information bits are recorded on both land track and groove track. To achieve a high areal density on disks, a groove structure having a narrow track pitch is preferred. In this case, it is imperative to control the optical and thermal cross talk between adjacent tracks. The optical cross-track cross talk can be reduced to an acceptable level by tuning the groove depth.[5] The thermal cross-track cross talk, however, becomes a serious problem during recording. Because of thermal diffusion from the central track and light absorption in the adjacent tracks, writing on the central track can partially erase the existing marks on the adjacent tracks.

To suppress thermal cross erasure, deep groove substrates have been suggested;[6] but the mechanism for thermal cross erasure is poorly understood. Moreover, it is observed that, on a disk with narrow track pitch, cross erasure on the land tracks is different from that on the groove tracks, and that the shapes of the written marks on the land tracks differ from those on the groove tracks.[7] These phenomena cannot be understood based on the scalar diffraction theory, which predicts that the diffraction of light from the land track is the same as that from the groove track.

In this article we report results of our computer simulation of the temperature distribution within phase-change LG disks under the influence of a focused laser beam. The absorption of optical energy in the medium is evaluated using rigorous vector diffraction calculations. The dependence of the temperature profiles on the wavelength of light, the state of polarization, and the geometry of the groove structure is discussed.

II. SIMULATION METHOD

Figure 1 is a diagram of our simulated system. A linearly polarized beam of light is brought to focus by an objective lens on an optical disk through its substrate. The incident beam is Gaussian, having its $1/e$ amplitude radius at the aperture of the lens. The substrate is grooved and coated with a conformal N-layer stack. Let X, Y, and Z be the axes of a Cartesian coordinate system, with the X axis perpendicular to the tracks (i.e., in the cross-track direction) and the Z axis parallel to the tracks, while the positive Y axis goes through the stack and into the substrate. For the particular problem addressed here the groove profile is trapezoidal in the XY plane, and invariant in the Z direction. We define $E_{\parallel}$ polarization as the case in which the electric field (hereafter referred to as E field) of the incident beam is parallel to the tracks (i.e., along the Z axis), and denote by $E_{\perp}$ the polarization when the E field is perpendicular to the tracks (along the X axis). To avoid any ambiguity in the definitions of land and groove, these are clearly marked in the diagram.

The simulation method described in this article consists of two steps. In the first step we calculate the electromagnetic field distribution and obtain the light absorption in the medium based on the vector diffraction theory. In the second step we obtain the temperature distribution in the medium by solving the thermal diffusion equation.

A. Rigorous vector diffraction

There are several numerical vector diffraction methods described in various publications. Most numerical methods are based on infinite periodic structures and plane-wave incidence. These methods include the integral method, the modal method, and the coordinate transformation method.[8–13] The diffraction of a focused beam can be simu-

[a]Electronic mail: cpeng@u.arizona.edu

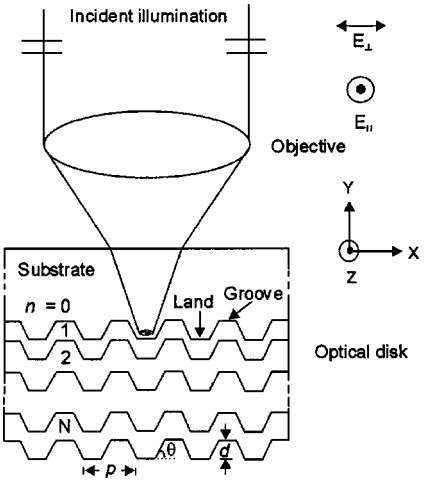

FIG. 1. Schematic diagram of the simulated optical system. A linearly polarized Gaussian beam of light is brought to focus onto a grooved optical disk by an objective lens. The number of layers in the disk is N. The groove has a trapezoidal shape with a period of p, a physical depth of d, and an inclination angle of θ.

lated by calculating separately each plane wave that comprises the incident field.[14,15] If the structure is finite and/or aperiodic, the integral or differential methods are usually employed.[16–22] Examples of the differential method are the finite difference method, finite element analysis, and the more recent finite difference in the time-domain and finite difference in the frequency-domain methods. We have chosen the finite difference in the time-domain (FDTD) method in our simulation because of its ability to model diffraction from complicated structures (e.g., random marks in the grooved tracks) encountered in the optical disk data storage system.

Because the FDTD method for numerical diffraction analysis is well described in the literature,[23] here we only give an outline of our FDTD algorithm. Our algorithm is formulated in a three-dimensional curvilinear coordinate system.[24] The coordinate surface conforms to the grooved surface. This eases the matching of the electromagnetic boundary conditions along the physical material boundaries in the disk, and also avoids the numerical errors introduced in the staircase approximation to the curved surface when a Cartesian coordinate system is utilized. Specifically, for the trapezoidal groove structure, if the groove profile in the XY plane is described by $y=a(x)$, the coordinate transformation for the curvilinear coordinate system $(u^1u^2u^3)$ can be expressed as

$$u^1=x, \quad u^2=y-a(x), \quad u^3=z. \tag{1}$$

In the trapezoidal groove structure studied, the sidewall may be very sharp. In this case, the E field and the magnetic field vary rapidly in the region of the sidewalls. To model the sharp sidewalls, a local fine mesh[25] in the sidewalls is used. The mesh along the u^1 axis on these regions can be denser than the coarse mesh on the tracks (flat regions) by a factor of an odd integer (3, 5, 7, or 9). The use of the curvilinear coordinate system and local fine mesh in the FDTD formulation enables us to make accurate and efficient computations.

The incident beam is introduced into the FDTD computation through an equivalent electric and magnetic current source on a source plane.[26] This source plane is located in the substrate (the incident medium), parallel to the XZ plane, and very close to the multilayer stack. We first calculate the incident E-field distribution at the focal plane by Fourier transforming the incident beam at the entrance pupil of the objective lens.[27] Then the incident E-field on the source-plane is obtained by a forward or backward propagation of the light from the focal-plane based on the direct Fresnel diffraction theory.[26] Having determined the E field on the source plane, the incident magnetic field can be computed from Maxwell's equations.

The incident light reaches the source plane at time $t=0$. It propagates and scatters in the multilayer stack. When the electromagnetic fields reach steady state (typically after 6–8 cycles of the monochromatic source), the E-field distribution in the disk is obtained. From the E fields, we compute the absorption of optical energy throughout the stack. The absorbed optical power is the main source of thermal energy in the disk.

B. Thermal diffusion within the disk

Denoting by T the temperature rise above ambient, and assuming that heat loss from the surface is proportional to T at the disk's surface, one obtains the following heat transfer equation:[28]

$$C_n\frac{\partial T}{\partial t}=K_n\nabla^2T+g, \quad n=0,1,2,...,N \tag{2}$$

with the following boundary conditions

$$T|_{x=\pm\infty}=0, \tag{3a}$$

$$T|_{y=+\infty}=0, \tag{3b}$$

$$\mathbf{n}\cdot\nabla T|_{\text{at surface}}=\gamma T|_{\text{at surface}}, \tag{3c}$$

$$T|_{z=\pm\infty}=0. \tag{3d}$$

Continuity conditions at the interface I_n between adjacent layers (nth and $n+1$ st) require that

$$T|_{I_n^+}=T|_{I_n^-}, \tag{3e}$$

$$\mathbf{n}\cdot(K_{n+1}\nabla T|_{I_n^+}-K_n\nabla T|_{I_n^-})=0. \tag{3f}$$

In Eqs. (2) and (3), C_n is the specific heat and K_n the thermal conductivity of the nth layer, g is the absorbed optical energy per unit time per unit volume converted to heat, $\mathbf{n}$ is a unit vector normal to the material boundary from nth layer to the $n+1$ st layer, (at the surface, $\mathbf{n}$ is outward from the surface), and γ is a constant that controls the rate of heat flow from the surface of the disk.

The thermal diffusion equation can be numerically solved using a finite-difference technique.[29] In the case of a flat substrate, a number of numerical procedures have been developed.[3,30–33] Exact solution of the heat diffusion equation has also been reported.[34,35] Here, because of the complexity of the problem, we use the alternating-direction im-

TABLE I. Period p, depth d, and sidewall inclination angle θ of the groove structure and light wavelength λ in the cases studied.

	$C1$	$C2$	$C3$	$C4$
p (μm)	0.72	0.72	0.72	1.14
d (nm)	50	100	100	80
θ (°)	63	76	54	63
λ (μm)	0.41	0.41	0.41	0.65

plicit finite-difference technique to solve Eqs. (2) and (3).[36] The numerical procedures are similar to those described in Ref. 3 for planar disks.

III. NUMERICAL RESULTS

In this section we apply our method of numerical analysis to four PC LG disks, and examine the effect of the groove geometry on the profiles of temperature distribution under focused beam illumination. Table I lists the characteristics of the groove structure in the four cases, $C1$, $C2$, $C3$, and $C4$. The wavelength λ of the incident beam in each case is also given in Table I. Throughout the section it is assumed that the objective lens has a numerical aperture NA$=0.65$ and the land track has the same width as the groove track.

From Table I we can categorize $C1-C4$ into two groups: $C1-C3$ and $C4$. The wavelength λ and track period p are the same in each group but different in the two groups: $\lambda=0.41$ μm and $p=0.72$ μm in $C1-C3$ while $\lambda=0.65$ μm and $p=1.14$ μm in $C4$. [The 0.41 μm light is expected to be used in the future generation digital versatile disk (DVD) drives, while the 0.65 μm light is used in the current DVD drives.[37]] In $C1-C3$, the groove has a different depth and/or inclination angle; they are designed for exploring how the groove geometry affects the profiles of temperature distribution. The track period and groove depth in $C4$ are scaled from those in $C1$ based on the wavelength: $p=0.72\times650/410\approx1.14$ μm, and $d=50\times650/410\approx80$ nm. (The sidewall inclination angle in $C4$ is equal to that in $C1$.) Case $C4$ is used to investigate the effect of wavelength on the profiles of temperature distribution.

All disks consist of four layers. The layer structures are the same in each group but different in the two groups. Table II shows the layer structures and Table III gives the material parameters used in the optical and thermal analyses. At normal incidence, the four disks absorb the same amount of optical energy (74%) if the substrates are flat (i.e., not grooved). In the thermal calculations, the disks are assumed to be stationary. The laser output power is 4 mW in $C1-C3$ and 7 mW in $C4$, starting at $t=0$ and lasting up to $t=100$ ns. In all thermal calculations, heat loss γ is assumed to be 100/cm. In our time interval, γ has little effect on the disk's temperature distribution.

TABLE II. Layer structure of the quadrilayer disk in $C1-C3$ and $C4$.

Substrate	Dielectric layer (nm)	PC layer (nm)	Dielectric layer (nm)	Reflector (nm)
$C1-C3$	135	18	21	100
$C4$	84	24	24	100

TABLE III. Numerical values for refractive index $\tilde{n}$, specific heat C, and thermal conductivity K of the quadrilayer stack.

	$\tilde{n}$ ($\lambda=0.41$ μm)	$\tilde{n}$ ($\lambda=0.65$ μm)	C (J/cm^3/°C)	K (W/cm/°C)
Substrate (polycarbonate)	1.54	1.58	1.7	0.0023
Dielectric layer ($ZnS-SiO_2$)	2.3	2.1	2.005	0.0058
PC layer ($Ge_2Sb_{2.3}Te_5$)	$1.78+i3.23$	$4.6+i4.2$	1.285	0.006
Reflector (Al alloy)	$0.5+i3.8$	$1.8+i6.0$	2.45	0.2

In the section we set $(u^1,u^3)=(0,0)$ at the center of the focused spot, and $u^2=0$ at the surface of the disk. In our curvilinear coordinate system, the u^1u^3 plane (i.e., $u^2=$constant) is conformal to the grooved structure.

A. Profiles of temperature distribution in $C1$

Figures 2–4 show the calculation results at $t=100$ ns in $C1$. Figure 2 shows plots of the temperature T versus x ($=u^1$) in the middle of storage layer ($u^2=140$ nm) and at $u^3=0$. It is seen that the temperature distribution is dependent on the state of polarization and on which track the focused spot is centered. T reaches its maximum at the center of the focused spot and then decreases with the distance off track. It is interesting to see that T has a local minimum in the sidewall and a side lobe on the nearest-neighbor tracks near the sidewalls. (In $C1$, the groove sidewalls start at $x\approx\pm167$ nm and end at $x\approx\pm193$ nm.) The peak value of T in the neighboring tracks is quite different for different polarizations and for different tracks. The $E_\perp$ polarization has a higher T tail on the neighboring tracks than the $E_\parallel$

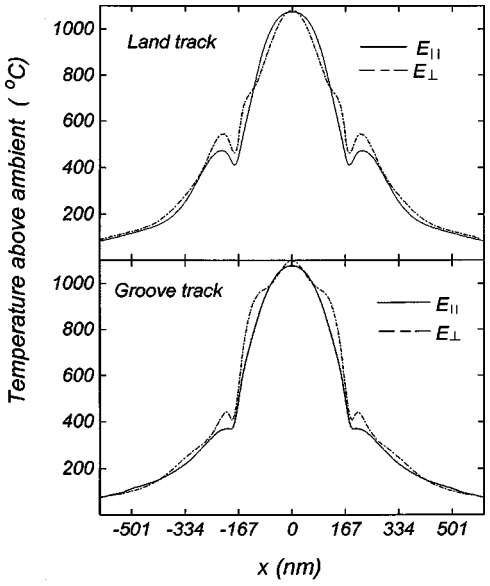

FIG. 2. Cross-track temperature distribution for both $E_\parallel$ and $E_\perp$ polarizations in $C1$. The focused beam is on a land or a groove track.

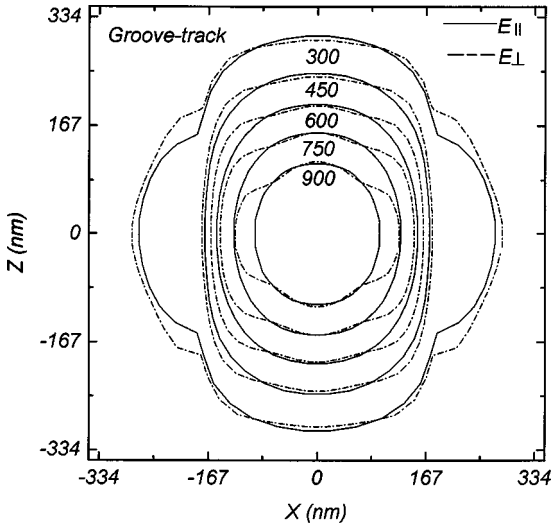

FIG. 3. Isotherms in the middle of the storage layer for both $E_\parallel$ and $E_\perp$ polarizations when the focused beam is on a groove track in $C1$. The temperature represented by each successive contour is 900, 750, 600, 450, and 300 °C.

polarization, and the thermal cross talk from a land track to its neighboring groove tracks is larger than the opposite case, i.e., the thermal cross talk from a groove track to its neighbor land tracks. These features will be seen more clearly further below.

Figures 3 and 4 display isothermal contours in the u^1u^3 plane at $u^2=140$ nm for both $E_\parallel$ and $E_\perp$ polarizations. Figure 3 is obtained when the beam is focused on a groove track, while Fig. 4 corresponds to a land track. There are ten contours on each diagram, five contours corresponding to the $E_\parallel$ polarization and the other five contours corresponding to the $E_\perp$ polarization. The temperatures represented by the five contours are 900, 750, 600, 450, and 300 °C. In Figs. 3 and 4, it is obvious that the isothermal contour is not circular for either $E_\parallel$ or $E_\perp$ polarization. For the $E_\parallel$ polarization, the

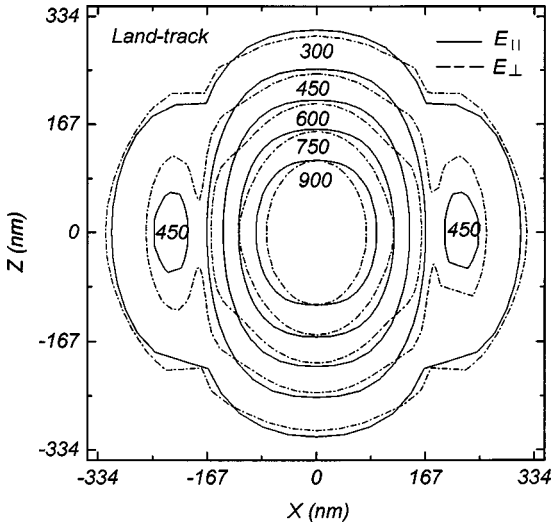

FIG. 4. Isotherms in the middle of the storage layer for both $E_\parallel$ and $E_\perp$ polarizations when the focused beam is on a land track in $C1$. The temperature represented by each successive contour is 900, 750, 600, 450, and 300 °C.

isothermal contours within the focused track tend to be elongated along the track (i.e., the Z direction in Fig. 1) on both land track and groove track. For the $E_\perp$ polarization, the behavior is more complicated. On the land track, the isothermal contours are also elongated along the track, while on the groove track, the isothermal contours near the edges of the track ($x\approx\pm167$ nm) are elongated along the track, but near the track center they are elongated in the cross-track direction.

From Figs. 3 and 4, it is also evident that the temperature gradients near the edges of the track are much higher than those near the track center. This means that the sidewalls confine the temperature profiles on the track to some extent, especially when the focused spot is on a groove track.

The currently used phase-change material in the DVD random-access memory system is $Ge_2Sb_{2.3}Te_5$ (GST) alloy. Its melting point is ~620 °C. In our simulations, the optical power was chosen to give $T\approx600$ °C near the edges of the track at $z\approx0$. In $C1$, $T\approx600$ °C at ($x\approx\pm155$ nm, $z\approx0$). In the GST layer, amorphous marks begin to crystallize at $T\sim400$ °C over time intervals of tens of nanoseconds. If $T>400$ °C in the neighboring tracks, the amorphous marks on these tracks may be partially erased. In Fig. 3, the isothermal contour at $T=450$ °C is almost confined on the focused groove track; therefore, the writing on a groove track will not affect the marks on its neighboring land tracks. On the other hand, the isothermal contour at $T=450$ °C in Fig. 4 falls on the nearest-neighbor tracks; the marks on the groove tracks may be partially erased while the central land track is being written.

When the laser is turned off, the hot spot will cool down. The cooling speed in the medium is dependent on the temperature distribution in the heating cycle. In PC recording, if the melted pool cools rapidly, the molten region transforms to an amorphous state. However, if the cooling rate is slow, the molten pool will crystallize. From Figs. 3 and 4, it is obvious that the temperature distribution around the isothermal contour at $T=600$ °C near the edges of the focused track is quite different between groove track and land track. On a land track, T is more uniform than that on a groove track. The cooling rate near the sidewalls of the land track is expected to be lower than that on the groove track, and, the quenched amorphous marks on a land track may be narrower than those on a groove track.

B. Profiles of temperature distribution in *C*2 and *C*3

The groove in $C2$ is twice as deep as in $C1$. Figures 5–7 show the calculated results. Figure 5 plots T versus x at $u^2=140$ nm and $u^3=0$, and Figs. 6 and 7 display the isothermal contours in the middle of the storage layer ($u^2=140$ nm). Once again the temperature distribution has side lobes in the neighbor tracks. Compared to $C1$, the isothermal contours in $C2$ are more elongated along the track and the profiles of temperature distribution are more confined to the focused track. In particular, when the focused beam is on a groove track, T is below 400 °C in the neighboring land tracks; thus writing on a groove track will not affect the marks on its neighboring land tracks. When the focused

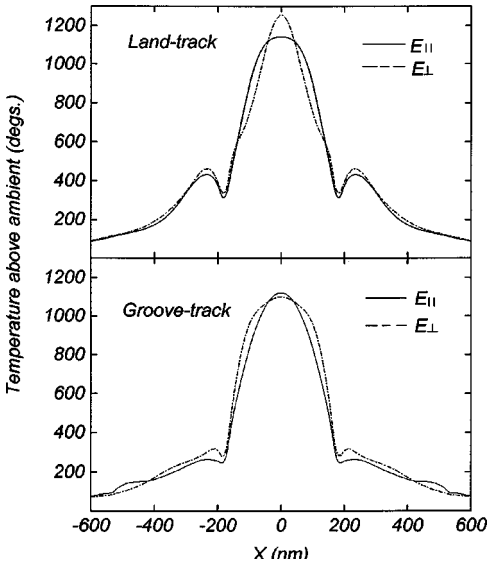

FIG. 5. Same as Fig. 2 but in $C2$.

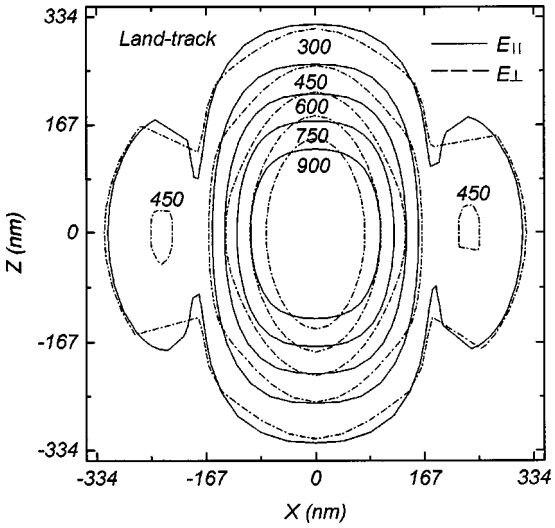

FIG. 7. Same as Fig. 5 but in $C2$.

beam is on a land track, the region $T>400\,^{\circ}\mathrm{C}$ exists only within a small area in the neighboring groove tracks for the $E_{\perp}$ polarization. The thermal cross-track cross talk is, therefore, substantially suppressed by the use of a deep groove. This is consistent with what was reported in Ref. 6.

Compared to $C1$, the isothermal contour at $T=600\,^{\circ}\mathrm{C}$ in $C2$ is further away from the edges of the track. This means that, if the same amount of power for writing is used in both $C2$ and $C1$, the recorded marks will be narrower in $C2$ than in $C1$. If we try to write marks having the same width as those in $C1$ by increasing the writing power in $C2$, the maximum T in $C2$ will reach about $\sim 1400\,^{\circ}\mathrm{C}$. So high a temperature in the storage layer may destroy the storage layer and degrade the cyclability of the medium.

Figures 8–10 show the calculated results for the case $C3$. The depth of the groove in $C3$ is the same as that in $C2$ but the sidewalls are much wider in $C3$. Figure 8 shows plots of T versus x, and Figs. 9 and 10 display the isothermal contours in the middle of the storage layer. The thermal behavior in $C3$ is similar to that in $C2$, but the thermal cross-track cross talk in $C3$ is slightly higher. Therefore, sharp sidewalls can also reduce the thermal cross-track cross talk to some extent, in agreement with experimental findings.[6]

C. Profiles of temperature distribution in *C4*

In $C4$, $\lambda=650$ nm, and the groove geometry is a scaled version of $C1$. Figures 11–13 show the calculated results. Figure 11 shows plots of T versus x at $u^2=140$ nm and $u^3=0$, while Figs. 12 and 13 display the isothermal contours in the middle of the storage layer ($u^2=140$ nm). On a land track, the maximum temperature T_m for both $E_{\parallel}$ and $E_{\perp}$ polarizations occurs at the center of the focused spot, but the magnitude of T_m for the $E_{\parallel}$ polarization is about 100 °C higher than that for $E_{\perp}$ polarization in $C4$. On a groove track, T_m for the $E_{\parallel}$ polarization also occurs at $(x,z)=(0,0)$, but for the $E_{\perp}$ polarization it occurs somewhere

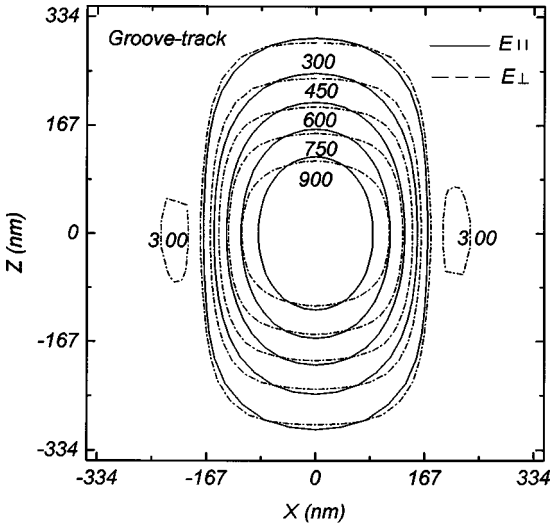

FIG. 6. Same as Fig. 3 but in $C2$.

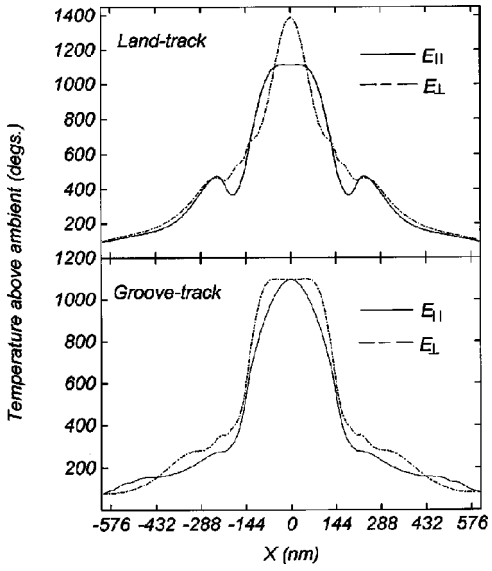

FIG. 8. Same as Fig. 2 but in $C3$.

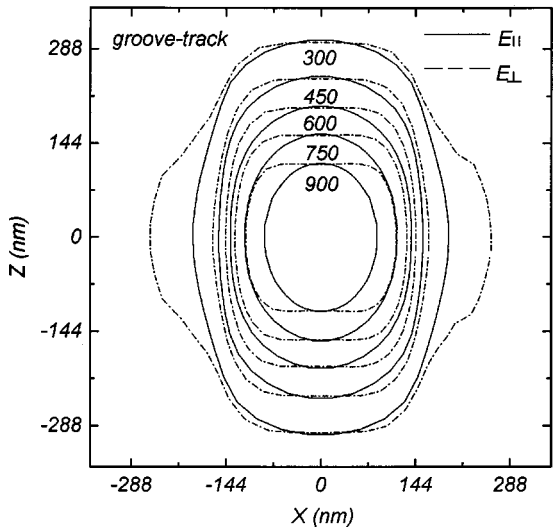

FIG. 9. Same as Fig. 3 but in $C3$.

between the track's centerline ($x=0$) and the sidewalls ($x=\pm 265\,\text{nm}$). This result differs from that in $C1$, and it is also unexpected from scalar diffraction theory. In the scalar theory, T_m always occurs at $(x,z)=(0,0)$ because the absorbed light in the medium is maximum at that point.

Similar to $C1$, T has a side lobe on the nearest-neighbor track near the groove sidewall ($x=\pm 305\,\text{nm}$). Relative to T_m, the peak value of T in the neighboring tracks is higher in $C4$ than in $C1$. So the thermal cross talk in $C4$ is more serious than in $C1$. This will be seen more clearly further below.

Comparing Figs. 12 and 13 with Figs. 3 and 4, it is obvious that the profiles of temperature distribution in $C4$ are quite different from those in $C1$. On a groove track in $C4$, the isothermal contour for $E_\parallel$ polarization is bent outward along the track, but for $E_\perp$ polarization it is bent inward. On a land track, the isothermal contours for both $E_\parallel$ and $E_\perp$ polarizations are curved outward along the track. In PC optical recording, circular polarization is usually used.

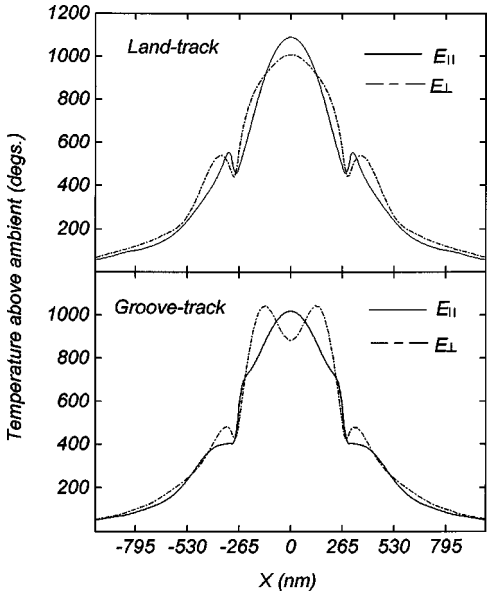

FIG. 11. Same as Fig. 2 but in $C4$.

We can approximate the temperature profile for the circular polarization as the average between $E_\parallel$ and $E_\perp$ polarizations. From Figs. 12 and 13 we expect the recorded marks on a groove track to have rectangular shapes with flat leading and trailing edges and those on a land track to have more or less elliptical shapes with outward curved edges.

In Fig. 12, the isothermal contour at 450 °C for $E_\perp$ polarization falls on the neighboring tracks ($|x|\geqslant 305\,\text{nm}$). This differs from the simulation in $C1$. Moreover, in Fig. 13, the isothermal contour at 450 °C is more extended to its neighboring groove tracks than in $C1$ (see Fig. 4). So the thermal cross-track cross talk seems to be more serious at longer wavelengths.

Figure 14 shows a transmission electron micrograph (TEM) of an actual PC optical disk. The groove period and depth of this disk are the same as those in $C4$. The wavelength of the incident light used in the write/read test is also

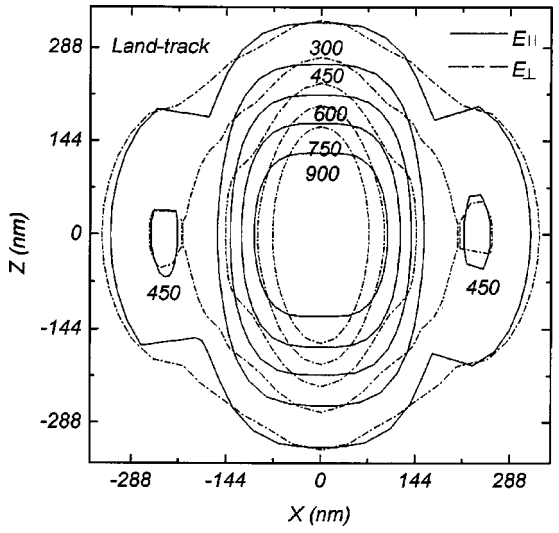

FIG. 10. Same as Fig. 5 but in $C3$.

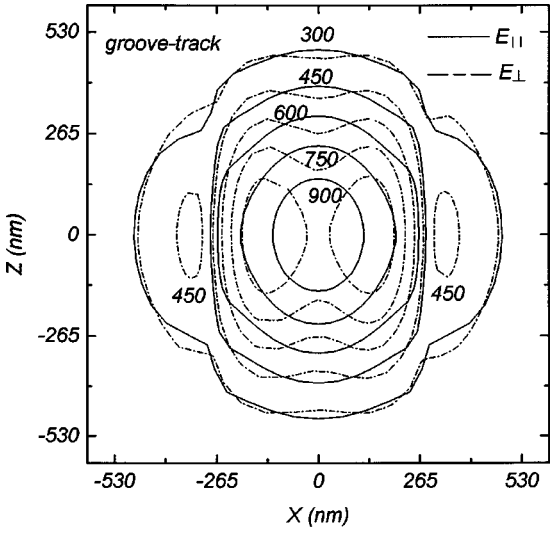

FIG. 12. Same as Fig. 3 but in $C4$.

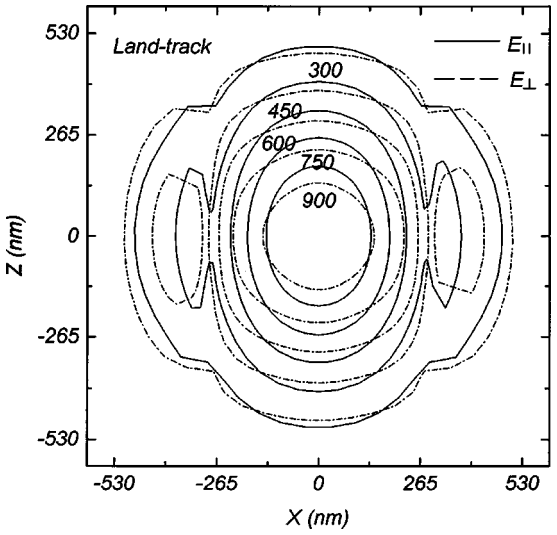

FIG. 13. Same as Fig. 5 but in $C4$.

similar to that used in $C4$. In the picture, the tracks that are slightly wider are the land tracks. It is seen that the marks on the groove tracks have rectangular shapes while the marks on the land tracks have elliptical and tear-dropped shapes. It is also seen that the marks on the groove tracks are more seriously cross erased than those on land tracks. These experimental results are in complete agreement with our theoretical results.

IV. CONCLUSIONS

We have investigated the three-dimensional temperature distribution in grooved optical disks under focused beam illumination. The electromagnetic fields in the medium are evaluated by numerically solving Maxwell's equations based on the FDTD technique, and the absorption of optical energy in different layers of the disk is thus obtained. The numerical solutions of the heat diffusion equation were obtained by the alternating direction implicit technique.

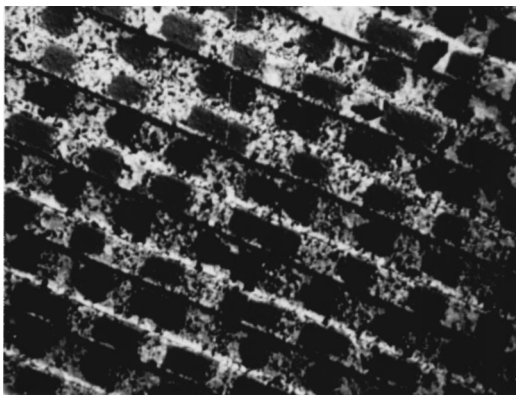

FIG. 14. TEM image of the recorded amorphous marks in a PC optical disk. The layer structure of the disk is 150 nm Al alloy/18 nm ZnS–SiO_2/25 nm $Ge_2Sb_{2.3}Te_5$/100 nm ZnS–SiO_2/polycarbonate substrate. In this disk, $p=1.14\ \mu$m, $d=80$ nm, and $\theta=55°$. The land tracks are 10% wider than the groove tracks. In the write/read test, $\lambda=0.650\ \mu$m and NA=0.6.

Calculations have demonstrated that the temperature distribution in the medium depends on the wavelength of light, the state of polarization, and the geometry of the groove structure. Deep grooves and sharp sidewalls can reduce thermal cross-track cross talk. For the cases studied, when the beam is focused on a groove track, we found the interaction between the $E_{\perp}$ electric field and the groove is mainly responsible for thermal cross-track cross talk. When the beam is focused on a land track, both $E_{\parallel}$ and $E_{\perp}$ polarizations can cause thermal cross-track cross talk, but the $E_{\perp}$ polarization gives slightly higher cross talk than the $E_{\parallel}$ polarization does.

ACKNOWLEDGMENTS

The authors thank Dr. B. K. Cheong and Dr. S. G. Kim of the Korea Institute of Science and Technology, Seoul, Korea for providing the TEM picture shown in Fig. 14.

[1] J. Feinleib, J. deNeufville, S. C. Moss, and S. R. Ovshinsky, Appl. Phys. Lett. **18**, 254 (1971).
[2] T. Ohta, K. Inoue, M. Uchida, K. Yoshioka, T. Akiyama, S. Furukawa, K. Nagata, and S. Nakamura, Jpn. J. Appl. Phys., Suppl. **28**, 123 (1989).
[3] C. Peng, L. Cheng, and M. Mansuripur, J. Appl. Phys. **82**, 4183 (1997).
[4] I. Satoh, S. Ohara, N. Akahira, and M. Takenaga, IEEE Trans. Magn. **34**, 337 (1998).
[5] N. Miyagawa, Y. Gotoh, E. Ohno, K. Nishiuchi, and N. Akahira, Jpn. J. Appl. Phys., Part 1 **32**, 5324 (1993).
[6] S. Morita, M. Nishiyama, and M. Furuta, Proc. SPIE **3109**, 167 (1997).
[7] B. K. Cheong, KIST, Seoul, Korea (private communication).
[8] A. Wirgin, Opt. Commun. **27**, 189 (1978).
[9] M. G. Moharam, E. B. Grann, D. A. Pommet, and T. K. Gaylord, J. Opt. Soc. Am. A **12**, 1068 (1995).
[10] G. Granet and B. Guizal, J. Opt. Soc. Am. A **13**, 1019 (1996).
[11] Lifeng Li, J. Opt. Soc. Am. A **14**, 2758 (1997).
[12] J. Chandezon, D. Maystre, and G. Raoult, J. Opt. (Paris) **11**, 235 (1980).
[13] L. Li, J. Chandezon, G. Granet, and J-P. Plumey, Appl. Opt. **38**, 304 (1999).
[14] K. Kobayashi, Jpn. J. Appl. Phys., Part 1 **32**, 3175 (1993).
[15] M. Mansuripur, Opt. Photonics News **38** (1997).
[16] D. S. Marx and D. Psaltis, J. Opt. Soc. Am. A **14**, 1268 (1997).
[17] J. G. Dil and B. A. J. Jacobs, J. Opt. Soc. Am. **69**, 950 (1979).
[18] T. Kojima and J. Ido, Electron. Commun. Jpn., Part 2: Electron. **74**, 11 (1991).
[19] K. Hirayama, E. N. Glytsis, and T. K. Gaylord, J. Opt. Soc. Am. A **14**, 907 (1997).
[20] J. B. Judkins, C. W. Haggans, and R. W. Ziolkowski, Appl. Opt. **35**, 2477 (1996).
[21] W. C. Liu and M. W. Kowarz, Appl. Opt. **38**, 3787 (1999).
[22] Y. Miyazaki, K. Tanaka, and R. Chiba, Jpn. J. Appl. Phys., Part 2 **38**, 1597 (1999).
[23] A. Taflove, *Computational Electrodynamics: The Finite-Difference Time-Domain Method* (Artech House, Boston, 1995), Chaps. 3–7.
[24] R. Holland, IEEE Trans. Nucl. Sci. **NS-30**, 4589 (1983).
[25] I. S. Kim and W. J. R. Hoefer, IEEE Trans. Microwave Theory Tech. **38**, 812 (1990).
[26] M. Mansuripur, J. Opt. Soc. Am. A **6**, 786 (1989).
[27] D. E. Merewether, R. Fisher, and F. W. Smith, IEEE Trans. Nucl. Sci. **NS-27**, 1829 (1980).
[28] H. S. Carslaw and J. C. Jaeger, *Conduction of Heat in Solids* (Oxford University Press, London, 1954).
[29] D. R. Croft and D. G. Iilley, *Heat Transfer Calculation Using Finite Difference Equations* (Applied Science, London, 1977).
[30] M. Mansuripur, G. A. N. Connell, and J. W. Goodman, Appl. Opt. **21**, 1106 (1982).
[31] R. J. Anderson, J. Appl. Phys. **64**, 6639 (1988).
[32] A. H. M. Holtslag, J. Appl. Phys. **66**, 1530 (1989).
[33] T. W. McDaniel, J. Magn. Soc. Jpn. **S1**, 251 (1996).
[34] W. A. McGahan and K. D. Cole, J. Appl. Phys. **72**, 1362 (1992).
[35] O. W. Shih, J. Appl. Phys. **75**, 4382 (1994).
[36] J. Douglas, Jr. and J. E. Guan, Numer. Math. **6**, 428 (1964).
[37] H. A. Wierenga, Proc. SPIE **3401**, 64 (1998).